Double Perovskite Structure: A Vibrational and Luminescence Investigation Providing a Perspective on Crystal Field Strength

ARTICLE *in* THE JOURNAL OF PHYSICAL CHEMISTRY A · JUNE 2012

Impact Factor: 2.69 · DOI: 10.1021/jp303626v · Source: PubMed

3 AUTHORS, INCLUDING:

Lixin Ning
Anhui Normal University
63 PUBLICATIONS **425** CITATIONS
SEE PROFILE

Peter Anthony Tanner
The Hong Kong Institute of Education
355 PUBLICATIONS **4,364** CITATIONS
SEE PROFILE

THE JOURNAL OF PHYSICAL CHEMISTRY A

Article

pubs.acs.org/JPCA

Double Perovskite Structure: A Vibrational and Luminescence Investigation Providing a Perspective on Crystal Field Strength

Wenyu Li,[†] Lixin Ning,[‡] and Peter A. Tanner*[,§]

[†]Department of Biology and Chemistry, City University of Hong Kong, Tat Chee Avenue, Kowloon, Hong Kong S.A.R., P. R. China

[‡]Department of Physics, Anhui Normal University, Wuhu, Anhui 241000, P. R. China

[§]Department of Science and Environmental Studies, Faculty of Liberal Arts and Social Sciences, The Hong Kong Institute of Education, Tai Po, Hong Kong S.A.R., P. R. China

ABSTRACT: The luminescence spectra of Eu^{3+} doped in a series of double perovskite lattices Ba_2LnMO_6 (Ln = Y, Gd; M = Nb, Ta) have been recorded at room temperature and 10 K. Together with FT-IR and FT-Raman spectra and aided by DFT vibrational energy calculations, assignments have been made for the crystal field levels of the ^5D_J (J = 0,1) and ^7F_J (J = 0−2) multiplets. The luminescence spectra are consistent with monoclinic symmetry of these systems. The crystal field parameters from the fitting of the energy level data set of Ba_2YNbO_6:Eu^{3+} enable the crystal field strength to be calculated, and the order of magnitude is $Cl^- < O^{2-} < F^-$ for the EuX_6^{n-} (n = 6 for halogen, 9 for oxide) moieties. For these systems, an empirical linear relationship between crystal field strength and electronegativity of ligand X has been found. By contrast, the nephelauxetic series from the depression of the Slater parameter F^2 is $Cl^- \approx O^{2-} > F^-$ > free ion for these systems.

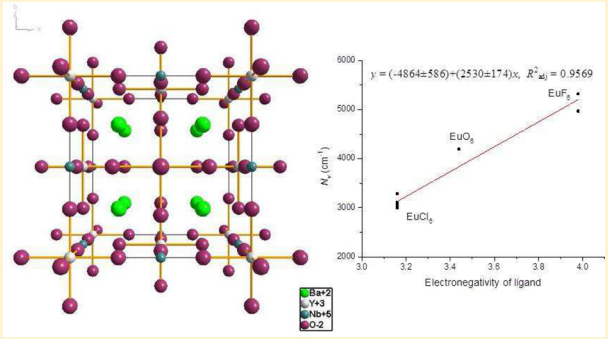

INTRODUCTION

The double perovskite structures of $Ba_2Ln(III)M(V)O_6$ comprise the large alkaline earth cation Ba^{2+} in the 12-coordinated A-site and the Ln^{3+} and M^{5+} cations located at octahedral sites in the lattice. Figure 1 shows the structure of Ba_2YNbO_6 plotted from the X-ray data from Fu and IJdo.[1] The NbO_6 and YO_6 octahedra link at corners in a three-dimensional framework. The Goldschmidt tolerance factor, $t = (r_A + r_O)/[\sqrt{2}(r_B + r_O)]$, of simple cubic perovskites ABO_3 is close to 1.0, whereas values between 0.75 and 1.0 are associated with distortion to tetragonal or lower symmetries. For double perovskites, the mean radius of Ln(III) and M(V) replaces r_B in the expression for the tolerance factor. The t values for eight $Ba_2Ln(III)M(V)O_6$ systems investigated by Lavat and Baran[2] were between 0.91 and 0.99, and they were assumed to be cubic ordered perovskites (space group $Fm\bar{3}m$, Z = 4) in that[2] and some other studies.[1,3−7] However, lower symmetry space groups have been proposed for these materials from other vibrational and X-ray diffraction studies. This is not unexpected, given the large difference in ionic radii between, for example, Nb^{5+}(VI) 0.64 Å and Y^{3+}(VI) 0.9 Å. The difficulties in establishing the structures of double perovskites have been discussed by Kennedy et al.[8]

The double perovskites have found various important applications, besides phosphors, in materials science. Nanorods of Ba_2YNbO_6 have been embedded in $YBa_2Cu_3O_7$ films in order to improve flux pinning in magnetic fields.[9] Other applications include a lead-free ultrasonic transducer for microelectronics, solid oxide fuel cells, and microwave tunable systems.[10−12] The band gaps of Ba_2YTaO_6 and Ba_2YNbO_6 are 4.6 and 3.8 eV, respectively.[13] The valence band is mainly composed of O(2p) orbitals, whereas the conduction band arises from the interaction between oxygen and transition metal t_{2g} orbitals for which the overlap increases when replacing a 4d ion with a more electropositive 5d ion.[14]

The luminescence of Ba_2GdNbO_6 doped with Eu^{3+} has been reported as a stick diagram by Blasse et al.[4] The local site symmetry of Eu^{3+} was assumed to be O_h, and the strong self-quenching of emission was attributed to exchange coupling via the NbO_6 moiety since the Eu−Eu separation is quite large (6 Å). An alternative explanation was offered by Qi et al.[15] in their study of the optical spectra of Ba_2NdNbO_6. A crystal disorder of ∼1% would be scarcely detectable by X-ray diffraction. In such a case, the separation of some Eu^{3+} ions would, however, be much smaller (3.6 Å) when occupying both of the Gd^{3+} and Nb^{3+} sites in Ba_2GdNbO_6, providing a self-quenching pathway.

The luminescence of several double perovskites doped with the probe ion Eu^{3+} has been investigated in the present study for a dual purpose. First, the interpretation of the low-temperature spectra of the Eu^{3+} ion in crystals is well-documented and can provide an indication of the site symmetry (or symmetries) of this impurity ion. This is simple because the electronic ground state ($^7F_0$) and the luminescent state ($^5D_0$) are both nondegenerate, and the observation of multiple $^5D_0$

Received: April 15, 2012
Revised: June 10, 2012
Published: June 17, 2012

   dx.doi.org/10.1021/jp303626v | J. Phys. Chem. A 2012, 116, 7337−7344

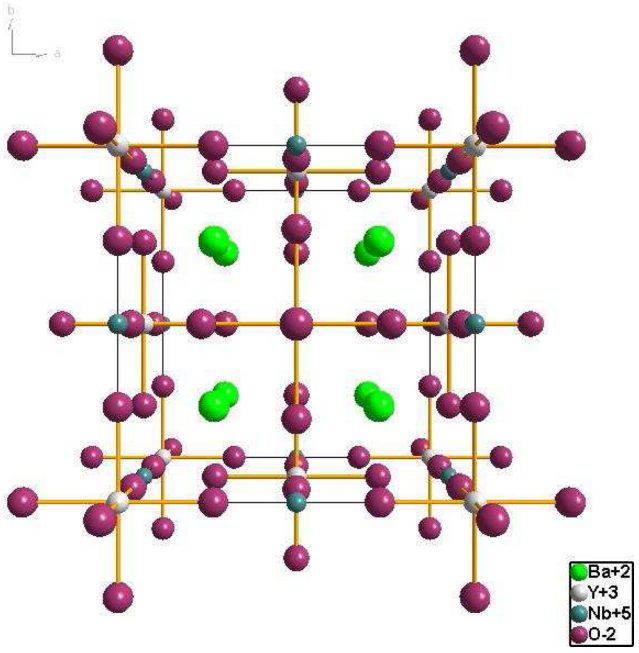

Figure 1. Structure of Ba_2YNbO_6 viewed along the c crystal axis (data from ref 1).

$\rightarrow {}^7F_0$ emission bands indicates the presence of multiple sites. The comparison of band intensities for the transitions enabled by magnetic dipole and forced electric dipole mechanisms, as well as the patterns of band splittings, provides additional site symmetry information. The description of the vibrational behavior of the crystal system using a first-principles calculation was useful for the understanding of the electronic spectra. The second motivation for this work utilized the (pseudo-) octahedral symmetry of the EuO_6^{9-} moiety, where theoretical parametrization is at a minimum, to gain a deeper understanding of metal−ligand interactions. The most concise way of summarizing such interactions lies in the crystal field strength parameter, subsequently defined. It transpires that the combination of results from this work with those from octahedral EuX_6^{3-} (X = Cl, F) systems provides a link between crystal field strength and electronegativity of X.

EXPERIMENTAL SECTION

The neat or doped double perovskites samples were prepared by a standard solid-state reaction method from the starting materials of $BaCO_3$ (Aldrich, 99.999%), Ln_2O_3 (Sigma-Aldrich, 99.999%), Nb_2O_5 (Strem, 99.999%), Ta_2O_5 (Strem, 99.999%) in stoichiometric amounts, and the dopants of Eu_2O_3 (Sigma-Aldrich, 99.999%). The masses of the starting materials Ba_2CO_3, Ta_2O_5, and Nb_2O_5 were 1.973, 1.105, and 1.329 g, respectively. The dopant ion concentrations were nominally 0.1 atom % to 10 atom % for Eu^{3+}. The appropriate mixture was ground, placed in a ceramic crucible, and prefired in air at 1000 °C for 12 h to decompose $BaCO_3$. The products were then reground, put into a platinum crucible, and sintered at 1200 °C for 24 h, and then at 1300 and 1400 °C for 48 h. In each step, the products were reground homogeneously.

X-ray powder diffraction (XRD) patterns were acquired on a Siemens D500 diffractometer using Cu Kα (λ = 1.54056 Å) at 40 kV and 30 mA with a scanning rate of 1.2° min^{-1} in the angle range from 10° to 80°. The FT-IR absorption spectra of all the related samples in discs or nujol mulls were recorded at room temperature in the range from 400 to 4000 cm^{-1} using a Nicolet FT-IR instrument with resolution 4 cm^{-1}. FT-Raman spectra of all the related samples in pellet form were recorded at room temperature by a Perkin-Elmer Spectrum 2000 spectrometer using a resolution of 4 cm^{-1}. Room temperature excitation and emission spectra (resolution ~3 nm) were recorded by a Jobin-Yvon Fluoromax-3 spectrofluorometer using a xenon lamp as the light source, and the signal was detected by a Hamamatsu R636 photomultiplier. High-resolution emission spectra were recorded at resolution between 2−4 cm^{-1} by an Acton 0.5 m monochromator having a 1200 groove mm^{-1} grating blazed at 500 nm, and a back-illuminated SpectruMM CCD detector, using an Optical Parametric Oscillator (Panther) pumped by the third harmonic of a Surelite Nd:YAG pulsed laser. The signal was collected at 90°. The sample was housed in an Oxford Instruments closed cycle cryostat.

THEORETICAL SECTION

Computational Method. The first-principles calculations were carried out using the DFT plane-wave code VASP[16] with the GGA-PBE exchange-correlation functional.[17] The $5s^25p^66s^2$ electrons on Ba, the $4s^24p^64d^15s^2$ electrons on Y, the $4s^24p^64d^45s^1$ electrons on Nb, and the $2s^22p^4$ electrons on O were treated as valence electrons in the calculations. The interaction between the valence electrons and the core was described using the projected augmented wave (PAW) method.[18,19] As a first step in determining the vibrational frequencies, the lattice and internal parameters of the Ba_2YNbO_6 primitive cell were optimized until the total forces on each ion were less than 10^{-4} eV $Å^{-1}$. The Γ-point vibrational frequencies were then computed by a finite-difference approach with a step size of 0.02 Å at 0 K. To ensure the convergence of results, the cutoff energy for the plain-wave basis was set to 400 eV, the criterion for electronic minimization was 10^{-6} eV, and a 6 × 6 × 6 Monkhorst-Pack *k*-point grid (63 irreducible **k** points) was used to sample the Brillouin zone.

RESULTS AND DISCUSSION

XRD Powder Patterns. Some powder X-ray diffraction patterns of the europium-doped barium double perovskites are displayed in Figure 2a. Two points are notable. First, all of the patterns are dominated by lines strongly resembling the primitive cubic perovskite but many lines are clearly split (a scale enlargement is provided in Figure 2b). This indicates that the room temperature crystal symmetries are lower than cubic. Second, there is a shift to smaller θ values for the more highly doped Eu^{3+} samples of Ba_2YMO_6 (M = Nb, Ta) resulting from a lattice expansion. For example, the peak at 30.2° in the 1% sample is at 30.6° in the 0.1% doped sample. This is consistent with the greater ionic radius of Eu^{3+}(VI) 0.947 Å compared with Y^{3+}(VI) 0.9 Å.

Vibrational Frequency Calculations. The optimization gave the values of the lattice parameter of Ba_2YNbO_6 as 8.4534 Å, and the internal parameter for oxygen as x = 0.2641. The corresponding experimental values are 8.4316 Å and 0.2665, respectively.[1]

In the space group $Fm\bar{3}m$, the irreducible representations of the **k** = 0 normal modes of vibration of Ba_2LnMO_6 systems transform as A_{1g} (R) + E_g (R) + $2T_{2g}$ (R) + T_{1g} (rot) + $4T_{1u}$ (IR) + T_{1u} (ac), where the notation in brackets denotes Raman or infrared activity, and rot and ac are rotational and acoustic

dx.doi.org/10.1021/jp303626v | J. Phys. Chem. A 2012, 116, 7337−7344

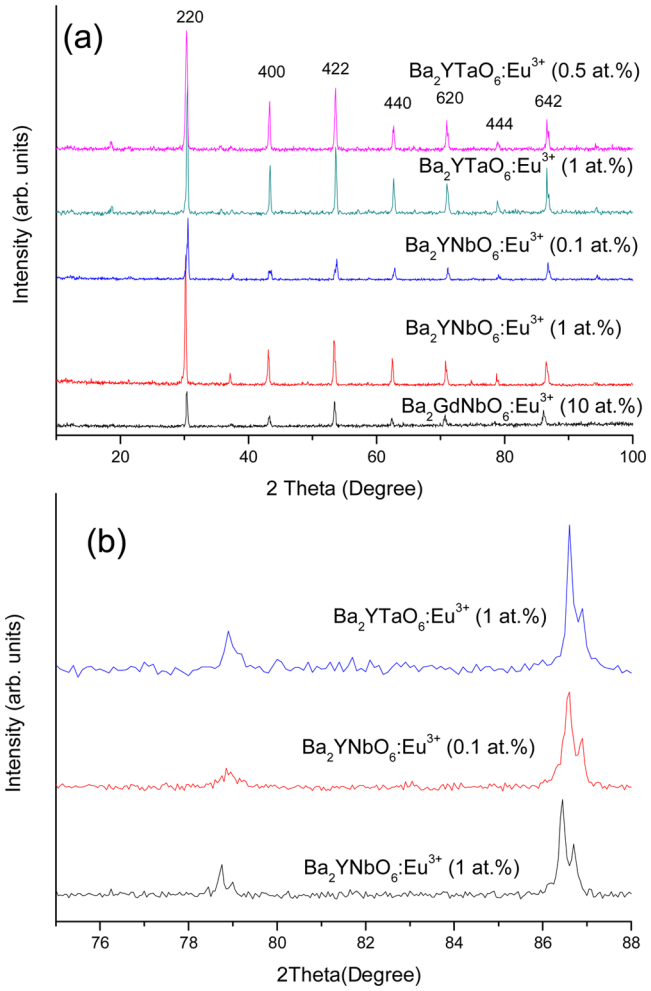

Figure 2. (a) Powder X-ray diffraction patterns of europium-doped barium double perovskites. A scale expansion is shown in panel b.

modes. The A_{1g} and E_g modes involve only oxygen motion, but barium ions move additionally for the T_{2g} mode. The A_{1g} mode is a breathing mode of the octahedron, whereas in the E_g mode, when four coplanar oxygens move toward the octahedron center, the other two oxygen ions move outward. The reported Raman spectrum of Ba_2MnWO_6 using 476 nm excitation is an excellent example of the expected 4-band Raman spectrum, with the A_{1g} peak much stronger than E_g.[7] Similar vibrational data for Ba_2GdSbO_6 are included in Table 1, column 8.[5]

The calculated vibrational energies for Ba_2YNbO_6, under the $Fm\bar{3}m$ space group, are listed in Table 1, column 3, with approximate mode descriptions given in column 2. Vibrational data for Ba_2YMO_6 from the present study are shown in Figure 3, and salient energies from Ba_2YNbO_6 are listed in Table 1, columns 4 (from our results) and 5 (from previous studies). The agreement with calculation is reasonable.

It is evident, however, from the IR and Raman spectra of Ba_2YNbO_6 that more bands are present than those expected for a cubic system.[1,20] The studies of Dias et al.[20−25] have arbitrarily fitted Lorentzian lines to the Raman spectra of double perovskites and then equated the number of lines to those predicted for certain symmetries. This fitting method has been criticized elsewhere[26,27] and described as mathematic rather than crystallographic. Symmetry lowering from the $Fm\bar{3}m$ space group can result from cation ordering in combination with the corner-linked tilting of the octahedral units and/or distortion of the octahedra.[22,28] Group−subgroup relationships establish the space group possibilities upon tilting of one axis to be from $Fm\bar{3}m$ to $I4/m$ or $P4/mnc$ and then to $P2_1/c$.[22,29] Rietveld analysis of the room temperature X-ray data of Ba_2LnNbO_6 (Ln = Gd, Eu) gave structures consistent with the $P2_1/n$ space group.[30]

The vibrational frequency calculation was also performed in the space group $I4/m$ for Ba_2YNbO_6, and we do not report this calculation in detail because two imaginary frequencies were then found. As expected, the vibrational degeneracies were removed but the gap between the calculated A_{1g} mode (795 cm^{-1}) and the E_g modes (551, 539 cm^{-1}) remained large. This is contrary to the experimental Raman spectra, where a feature at 747 cm^{-1} is observed. It therefore does not appear that this band is related to the descent in symmetry to $I4/m$, but presumably it arises in the descent to lower symmetry. Two previous reports may also be relevant. Yashima et al.[31] observed a peak at 811 cm^{-1} in the Raman spectrum of $YNbO_4$, but the frequency was rather lower (at 778 cm^{-1}) in Y_3NbO_7. In the latter compound, and in the defect fluorite solid solutions $Y_{100-x}Nb_xO_{150+x}$ ($20 < x < 25$), it was suggested that disorder exists so that some Nb ions substitute for Y and O substitutes for oxygen vacancy. Second, from the Raman and synchrotron X-ray diffraction study of Ba_2YTaO_6, Zhou et al.[32] provided evidence that the peak at 747 cm^{-1} in Ba_2YTaO_6 increases in intensity after ball-milling the sample, which serves to create

Table 1. Vibrational Modes and Their Calculated and Experimental Energies in Some Double Perovskite Systems[a]

		Ba_2YNbO_6[c]					
O_h symmetry mode	approx. description[b]	calcd	obs	obs[2,20]	Ba_2YTaO_6	Ba_2GdNbO_6	Ba_2GdSbO_6[5]
A_g	Nb−O sym str	804	811 R	800 R	841 R	810 R	762 R
E_g	O−Nb−O str	551	538 R	534 R	562 R	537 R	575 R
T_{1u}	Nb−O antisym str	525	556 IR	556 IR	567 IR	530 IR	627 IR
T_{2g}	O−Nb−O bend	363	384 R	372 R	390 R	380 R	375 R
T_{1u}	Y−O antisym str	303	337 IR	337 IR			
T_{1u}	O−Y−O bend	192					
T_{2u}	O−Y−O bend	163					
T_{2g}	lattice	95		95 R			105 R
T_{1u}	lattice	92					
T_{1u}	acoustic						

[a]Unless indicated otherwise, the data are from the present study. [b]Sym, symmetric; str, stretch; antisym, antisymmetric. [c]Calcd, calculated; Obs, observed; R, Raman; IR, infrared.

dx.doi.org/10.1021/jp303626v | J. Phys. Chem. A 2012, 116, 7337−7344

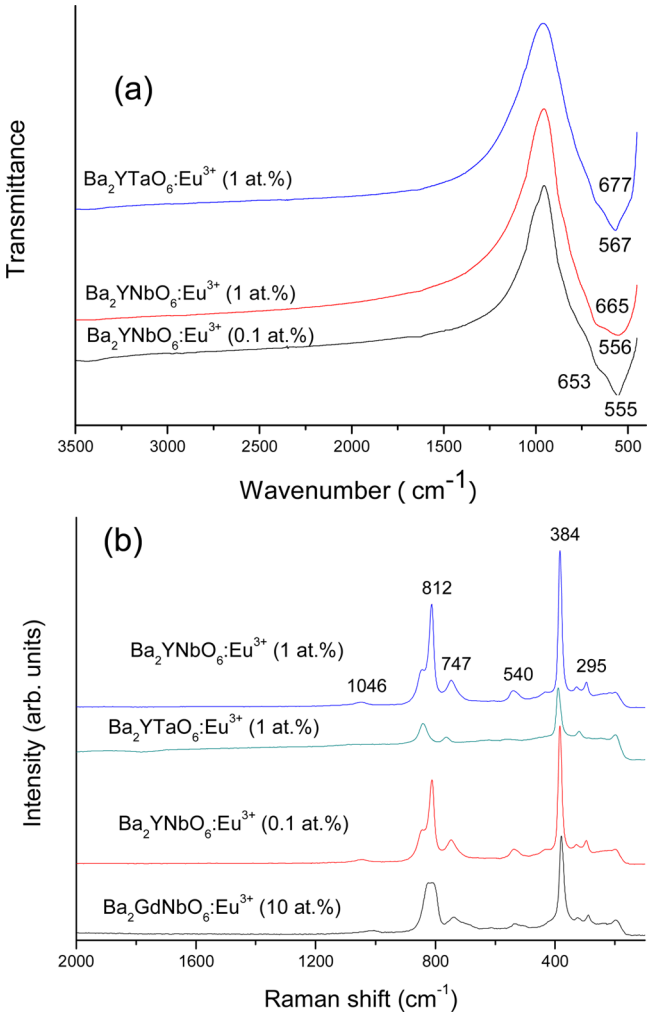

Figure 3. Infrared (a) and Raman (b) spectra of Eu^{3+}-doped barium double perovskites at room temperature.

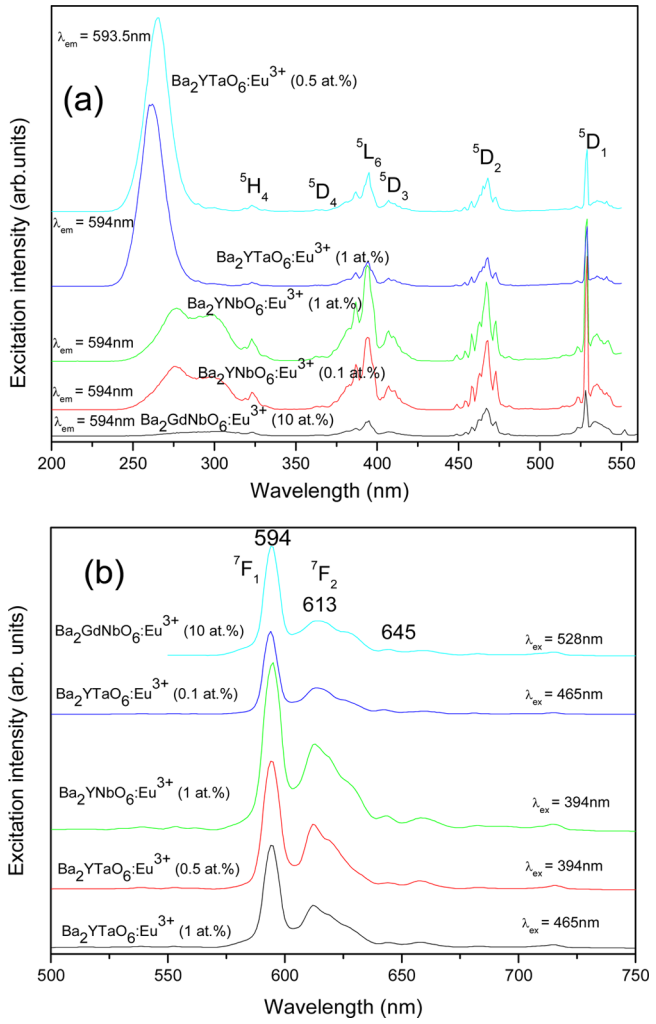

Figure 4. Room temperature excitation (a) and emission (b) spectra of europium-doped double perovskites. Some of the terminal multiplet terms are indicated. The excitation is from $^7F_{0,1}$, whereas the emission is from $^5D_0$.

defect sites. This band was in fact assigned to the cubic E_g mode by these authors, which is considered to be unlikely from our calculations. The presence of disorder was found to inhibit the cubic-tetragonal transition at ~260 K in this material, and it was concluded that prolonged sample heating is necessary in order to establish long-range ordering of Ta and Y atoms. Hammink et al. gave a similar conclusion for the ordering between In^{3+} and Ta^{5+} cations in Ba_2InTaO_6 from Rietveld profile analysis of X-ray diffraction data,[26] and a high degree of short-range order was proposed for the Fe/Mo cation antisite defects in Sr_2FeMoO_6.[27]

Room Temperature Electronic Spectra. The room temperature excitation and emission spectra of some double perovskites doped with Eu^{3+} are shown in Figure 4, and all spectra show similar characteristics for the Eu^{3+} transitions. Some of the terminal multiplet terms are marked in Figure 4a. The absorption occurs from the $^7F_0$ and $^7F_1$ multiplets at room temperature. The spectral resolution is not adequate for band assignments of crystal field levels. The emission spectra (Figure 4b) exhibit maximum intensity at ~595 nm and differ considerably from those reported by Xiao and Yan[33] but are consistent with the emission spectrum of Blasse et al.[4] and Yu et al.[34] The room temperature charge transfer excitation and emission bands of Ba_2YNbO_6 and Ba_2YTaO_6 have been reported at 314, 263 nm (excitation) and 530, 390 nm (emission), respectively.[13] The maxima in the room temperature excitation spectra (Figure 3a) are at 262 nm and 277, 305 nm, respectively for Ta−O and Nb−O charge transfer bands, but the corresponding emission bands are almost quenched via energy transfer to Eu^{3+}. Yu et al.[34] have reported the room temperature $^5D_0$ lifetime in Ba_2GdNbO_6:Eu (10 at. %) to be 2.26 ms. The radiative (natural) lifetime of the $^5D_0$ state may be estimated by the comparison of the integrated areas of emission, $I[^5D_0 \rightarrow {}^7F_1]/I[^5D_0 \rightarrow {}^7F_J;\ J = 0{-}6]$ and taking the spontaneous emission probability of $^5D_0 \rightarrow {}^7F_1$ to be 14.65 s^{-1} in vacuo.[35] By assuming a refractive index of 2.1 [36] and employing the integrated areas at room temperature, the $^5D_0$ natural lifetime is then estimated to be 7.4 ms in Ba_2GdNbO_6:Eu^{3+} (10 at. %). By using the observed lifetime above, this infers an internal quantum efficiency of 31%.

The CIE coordinates of Ba_2YNbO_6:Eu^{3+} (0.1 at. %) emission spectrum, excited by 459.7 nm radiation at 100 K, are (0.602, 0.398), similar to those of the Ba_2YNbO_6:Eu^{3+} (1 at. %) spectrum excited by 467 nm radiation at room temperature (0.612, 0.386). These color coordinates lie at the edge of the color gamut on the chromaticity diagram, representing maximum saturation for orange-red.

dx.doi.org/10.1021/jp303626v | J. Phys. Chem. A 2012, 116, 7337−7344

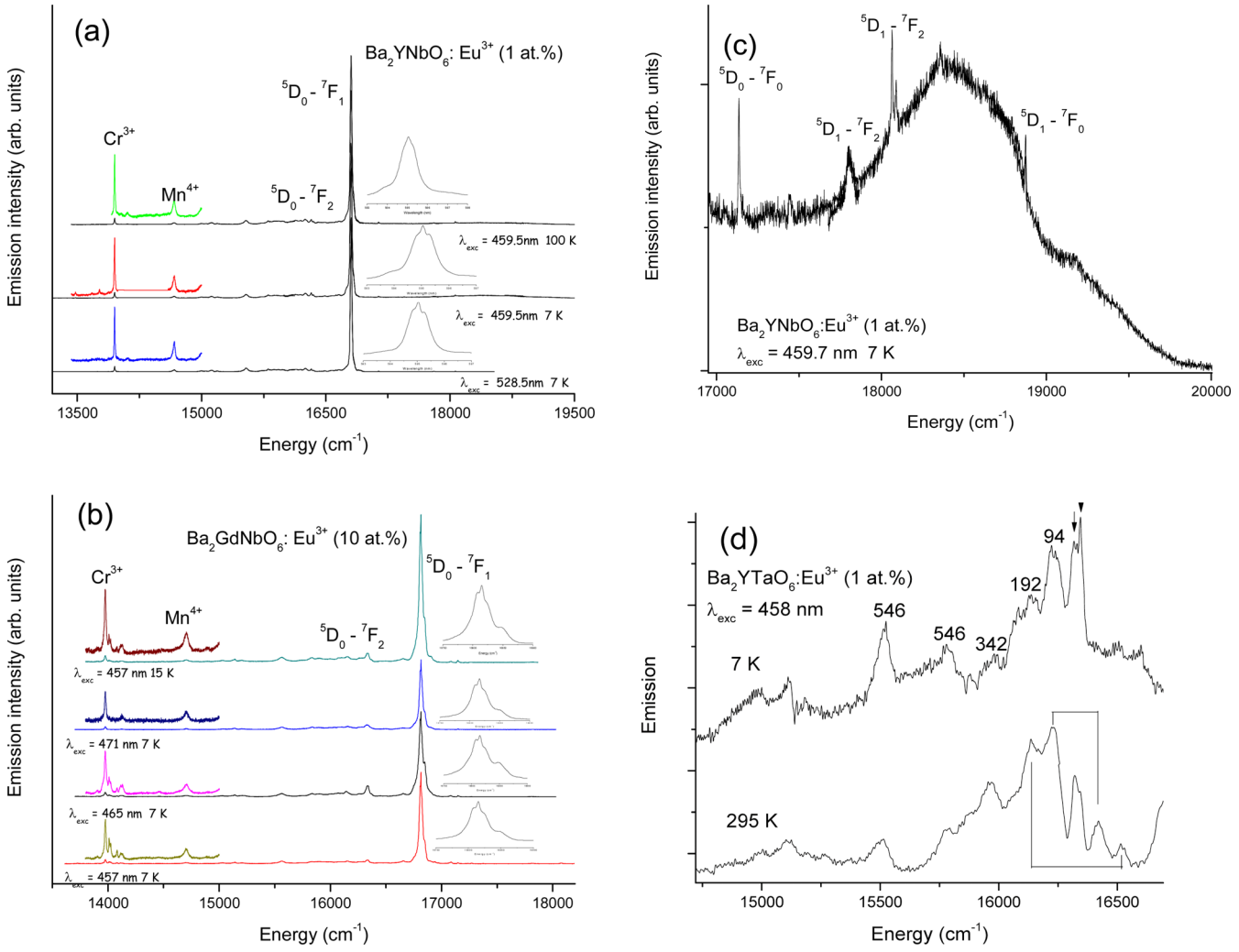

Figure 5. Emission spectra of Eu^{3+}-doped double perovskites: (a,b) 10 K survey spectra of Ba_2YNbO_6:Eu^{3+} and Ba_2GdNbO_6:Eu^{3+}. Scale expansions of the $^5D_0 \rightarrow {}^7F_1$ bands are indicated; (c) region between 20 000 and 16 950 cm^{-1} of the 10 K Ba_2YNbO_6 spectrum on an expanded scale; (d) region between 16 670 and 14 730 cm^{-1} of the 10 and 295 K Ba_2YTaO_6 spectra on an expanded scale.

Low Temperature Electronic Spectra. The survey 10 K emission spectra of the Eu^{3+}-doped Ba_2LnNbO_6 (Ln = Y,Gd) systems are displayed in Figure 5a,b, employing energy scales. In each case, the $^5D_0 \rightarrow {}^7F_1$ magnetic dipole transition at ~595 nm (~16 800 cm^{-1}) dominates the entire spectrum. The insets in these figures show that this band is split into 3 components in each case, so that the highest possible site symmetry point group of Eu^{3+} comprises a C_2 axis. The relative intensities of the $^5D_0 \rightarrow {}^7F_1$ and $^5D_0 \rightarrow {}^7F_2$ bands show a sharp contrast to those of Ba_2LaNbO_6 doped with Eu^{3+}, where the latter features dominate.[37] In the present case, the dominance of $^5D_0 \rightarrow {}^7F_1$ indicates centrosymmetry, or very near centrosymmetry, for the EuO_6^{9-} moiety. The Eu^{3+} site symmetry alternatives are then C_{2h} or C_i. Unfortunately, just as in the emission spectra of Ba_2LaNbO_6,[37] the lower energy regions of the emission spectra of our samples comprise bands due to the luminescence of Mn^{4+} and Cr^{3+} which are not further reported. We were therefore unable to measure the Eu^{3+}emission in these spectral regions. Our analysis is therefore curtailed to the $^5D_{0,1} \rightarrow {}^7F_{0,1,2}$ transitions of Eu^{3+}.

Figure 5c shows the enlargement of the 459.7 nm excited 7 K spectrum of Ba_2YNbO_6:Eu^{3+} (1 at. %) between 20 000 and 16 950 cm^{-1}. Some sharp features due to Eu^{3+} overlay the broadband structure peaking at ~18 430 cm^{-1} (542 nm) corresponding to the Nb−O charge transfer emission. The highest energy band, at 18 875 cm^{-1}, corresponds to the $^5D_1 \rightarrow {}^7F_0$ transition, whereas bands due to $^5D_1 \rightarrow {}^7F_2$ are observed at 18 088, 18 064, and 17 803 cm^{-1}. The appearance of the $^5D_0 \rightarrow {}^7F_0$ band at 17 136 cm^{-1} indicates a slight deviation from centrosymmetry.

The emission spectra of Ba_2YTaO_6:Eu^{3+} between 16 675 and 14 730 cm^{-1} at 7 K and room temperature are shown in Figure 5d. The higher energy bands are associated with the $^5D_0 \rightarrow {}^7F_2$ transition. The correspondence of Stokes and anti-Stokes features is indicated in the room temperature spectrum, and this enables the vibrational assignments shown in the 7 K spectrum to be made. The inferred zero phonon lines of this transition are masked by the nearby variable-intensity bands, indicated by vertical arrows in the upper figure. These features are associated with forced electric dipole transitions at Eu^{3+}defect sites. The assigned vibration at 94 cm^{-1} in the upper figure is associated with the T_{2g}/T_{1u} modes, whereas the 192, 342, and 546 cm^{-1} vibrations correspond to T_{1u} modes. The latter energy is rather smaller than that in the infrared spectrum of bulk Ba_2YTaO_6 since it shows, according to the local luminescent probe Eu^{3+}, a slight weakening of the Ta−O

dx.doi.org/10.1021/jp303626v | J. Phys. Chem. A 2012, 116, 7337−7344

bond when the cation Y^{3+} is replaced by the 5.2% larger Eu^{3+}ion.

Crystal Field Calculations. The deduced energy levels of Eu^{3+} are fairly similar for the Ba_2LnMO_6:Eu^{3+} systems investigated herein so that only the data for the Ba_2YNbO_6 host is discussed. The calculation of electronic energy levels for the $4f^6$ configuration employed the f-shell programs of Professor M. F. Reid in which the energy levels were derived by simultaneous diagonalization of various parametrized interaction Hamiltonians. The details of such calculations can be found in ref 38. Only the energy level values for the ^7F_J (J = 0−2) and ^5D_J (J = 0,1) have been determined by experiment. For Ba_2YNbO_6, the determined energies are listed in Table 2, from the experimental values of 325, 332, and 338 cm^{-1} ($^7F_1$) and 785, 809, and 1067 ($^7F_2$). The conversion of the nondegenerate crystal field level energies to those appropriate for O_h symmetry was made by using the level barycenters so that only 6 experimental energy levels are available (Table 2). The octahedral point group (O_h) of the rare-earth site imposes two independent crystal field parameters, B_{40} and B_{60}. The values of the Slater parameters, F^2, for Coulomb interaction between the 4f electrons, ζ(4f) for the spin−orbit interaction, and the two crystal-field parameters were varied simultaneously within certain allowed ranges and optimized until the best agreement was obtained between the calculated and observed energy levels. Thus, the total number of variable parameters in the fit was equal to 4. The ratios F^4/F^2 (= 0.77235) and F^6/F^2 (= 0.54016) and the values of the configuration interaction parameters, α, β, and γ, as well as the k = 0 magnetic interaction parameters M^k (M^2 = 0.56 M^0; M^4 = 0.38 M^0) were held fixed and equal to those of the elpasolite compound $Cs_2NaEuCl_6$.[39] The resulting parameter values are listed in column 2 of Table 3, and the calculated $4f^6$ crystal field energy levels are given in column 2 of Table 2. It is noted that the parameter values for Eu^{3+} in Ba_2YNbO_6 apply to a small data set comprising the ^5D_J (J = 0,1) and ^7F_J (J = 0−2) multiplets. Nevertheless, the values of the Slater and spin−orbit coupling parameters represent the lowest ones in the table. The comparison of the F^2 and ζ(4f) values in Table 3 with those of the free Eu^{3+} ion, namely, 113 551 cm^{-1} and 1414 cm^{-1},[40,41] respectively, shows decreases of ∼30% and 7%, respectively. Such decreases are normally associated with nephelauxetic effects, as an expansion of the 4f electron cloud in a crystal. The expected nephelauxetic effect (i.e., depression of F^2) for the centroid shift of EuX_6 is Cl^- > O^{2-} > F^- > free ion,[42] and in the present case, $Cl^- \approx O^{2-}$. The nephelauxetic effect is notably weaker for Eu^{3+} in 12-coordination ($Cs_2NaEu(NO_2)_6$, Table 2) due to the considerably longer Eu−O bond distance.[45] The Eu−O bond distances in the $Eu(O_2N)_6^{3-}$ and EuO_6^{9-} moieties are 2.65 ± 0.2 Å[45] and 2.247 Å.[1]

The parameters B_{20} and B_{22} of the Hamiltonian $B_{20}C_{20} + B_{22}(C_{22} + C_{2-2})$ are responsible for the splitting of the $^7F_1$ (O_h) J = 1 level. On the basis of the symmetry considerations, this level will split into the $|J, M_J\rangle$ states $|1,0\rangle$, $|1,1\rangle - |1,-1\rangle$, and $|1,1\rangle + |1,-1\rangle$ (with normalization factors neglected). The relative energies and the energy ordering of these states depend on the magnitude and sign of the B_{20} and B_{22} parameters. The use of

Table 2. Energy Level Fit for Eu^{3+} Levels in Ba_2YNbO_6

$^{2S+1}L_J$ Γ	calcd[a]	exptl[b]	calcd − exptl
$^7F_0$ A	0	0	0
$^7F_1$ T	350	332	18
$^7F_2$ E	803	797	6
T	1070	1067	3
$^7F_3$ A	1735		
T	1921		
T	1950		
$^7F_4$ T	2604		
E	2906		
T	3048		
A	3155		
$^7F_5$ T	3731		
E	3759		
T	3828		
T	4088		
$^7F_6$ E	4744		
T	4780		
A	4846		
T	5316		
T	5346		
A	5376		
$^5D_0$ A	17152	17137	15
$^5D_1$ T	18863	18872	−10

[a]Calculated energy using the parameters in Table 3. [b]Corrected barycenter energy.

Table 3. Energy Parameter Values for Some Eu^{3+} Crystalline Systems[a]

	value (cm^{-1})			
	Ba_2YNbO_6:Eu^{3+}[b]	$Cs_2NaEuCl_6$	Cs_2NaYF_6:Eu^{3+}	$Cs_2NaEu(NO_2)_6$[b]
parameter	$NbO_6(O_h)$	$EuCl_6(O_h)$[39]	$EuF_6(O_h)$[43]	$EuO_{12}(T_h)$[44,45]
F^2	79186	79688(109)	83789(50)	82149
ζ(4f)	1308	1331(2)	1323(13)	1331
B_{40}	2707	1936(23)	3138(65)	−327
B_{60}	88	245(16)	382(42)	−260
B_{62}				−1680
N	6	77	21	22
n_p	4	11	4	7
δ_2	10.5	14.2	31.5	18.9

[a]The parameter values (in cm^{-1}): α = 27.7, β = −1272, γ = 1461, M^0 = 2.13, P^0 = 195, T^2 = 278, T^3 = 40, T^4 = 40, T^6 = −546, T^7 = 244, T^8 = 241, were fixed with the values taken from the fit of $Cs_2NaEuCl_6$. The ratios F^4/F^2 (= 0.77235) and F^6/F^2 (= 0.54016) were held fixed. N number of energy levels fitted; n_p number of adjustable parameters; δ_2 mean deviation of fit. Values in parentheses indicate uncertainties. [b]No uncertanties available.

dx.doi.org/10.1021/jp303626v | J. Phys. Chem. A 2012, 116, 7337−7344

parameter values $B_{20} = -37.3$ cm^{-1} and $B_{22} = -15.3$ cm^{-1} provides calculated $^7F_1$ energies (in cm^{-1}) of 341, 350, and 359, which are in the best agreement with the experimental results for Ba_2YNbO_6:Eu^{3+}. These parameter values are small when compared with B_{40} and indicate a small deviation from octahedral symmetry. Fixing the magnitudes of these parameter values but changing their signs gave the following conclusions. First, the signs of B_{20} and B_{22} have no influence on the level energies but do affect the character of the levels. That is, only from the experimental energies, the signs of the B_{20} and B_{22} parameters cannot be uniquely determined. Second, if B_{20} is negative, then ^7F $|1\ 0\rangle$ is the lowest state, whereas if B_{20} is positive, then ^7F $|1,0\rangle$ is the highest state. The sign of B_{22} decides the relative ordering of the $|1,1\rangle - |1,-1\rangle$ and $|1,1\rangle + |1,-1\rangle$ states.

A comparison of the calculated parameters can be made with those from some related previous studies. Wakeshima et al.[46] have stated, from magnetic susceptibility measurements, that the spin−orbit coupling constant for Eu^{3+} in Ba_2EuIrO_6 is 364 cm^{-1}. This value is in fact the calculated energy difference between the $^7F_0$ and $^7F_1$ multiplet states and in the absence of J-mixing would be equal to $\zeta(4f)/6$. Zhou et al.[13] have investigated the luminescence of Ba_2YMO_6 (M = Nb, Ta) doped with Yb^{3+} at room temperature. The spectra were assigned to Yb^{3+} at an octahedral site in this host. From the experimental determination of four energy levels of Yb^{3+} in Ba_2YNbO_6, the crystal field parameters were calculated as (in cm^{-1}) $B_{40} = 2165$, $B_{60} = 122$. These values are in reasonable agreement with the present study.

The scalar crystal field strength parameter, which measures the average ligand field effect, is defined by Auzel and Malta as[47,48]

$$N_v = \left[\sum_{k,q} \frac{4\pi}{2k+1} B_{k,q}^2\right]^{1/2}$$

It has been demonstrated that the relationship between N_v and the maximum crystal field splitting of a multiplet is linear.[47,48] For lanthanide ions, the crystal field strength has been proposed to follow a different trend from the nephelauxetic series, namely, $Cl^- < F^- < O^{2-}$.[42] Some values of N_v for EuX_6 (X = Cl, F, O) and EuO_{12} systems are listed in Table 4. Variations in the value of N_v for a given system are

Table 4. Scalar Crystal Field Strengths of Some High Symmetry Eu^{3+} Systems

system	moiety (symmetry)	range of N_v (cm^{-1})	refs
Cs_2NaYF_6:Eu^{3+}	EuF_6 (O_h)	4970−5317	43, 49
$BaYNbO_6$:Eu^{3+}	EuO_6 (O_h)	4195	this work
$Cs_2NaEuCl_6$	$EuCl_6$ (O_h)	3000−3293	39, 50
$Cs_2NaEu(NO_2)_6$	EuO_{12} (T_h)	2447	44

mainly due to (i) the different number of crystal field levels fitted in the energy parametrization, due to the variation of crystal field parameters for different multiplet terms; (ii) fitting errors, due to holding certain parameters at assumed constant values. The above trend is not followed since N_v is clearly the greatest for the fluoride system. Herein, we have found another relationship for N_v. It is found that N_v is linearly related to the electronegativity of X for the EuX_6 systems (Figure 6) with the equation given in the figure. The rather scarce crystal field data sets reported from the electronic spectra of $LnBr_6^{3-}$

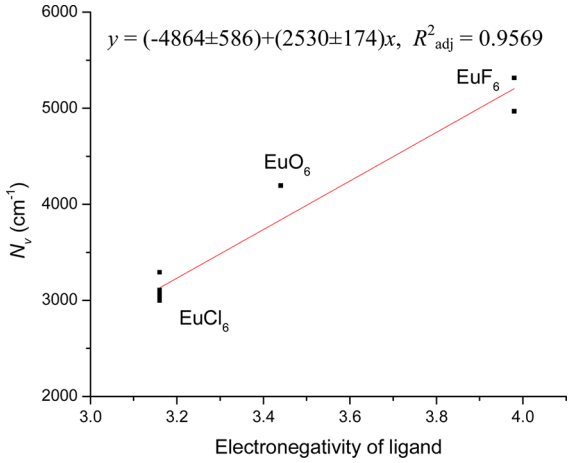

Figure 6. Empirical relationship between crystal field strength and electronegativity of X in EuX_6.

systems[50,51] do not show a consistent trend across the lanthanide series. The value of N_v for Ln = Tb is 2323 cm^{-1}.[51] Using the equation in Figure 6 together with the electronegativity 2.96 for Br, the predicted value of N_v for $EuBr_6^{3-}$ (expected to be greater) is 2625 cm^{-1} with a ∼6% fitting error.

Comparison with Ab initio Calculation. Visser et al. have performed a molecular open shell configuration interaction calculation using the Dirac−Coulomb Hamiltonian for the $4f^6$ configuration of Eu^{3+} in octahedral symmetry for the EuO_6^{9-} moiety.[52] It was found necessary to utilize an embedded cluster model in order to simulate the crystal field splittings. The calculated energies of some levels were (in cm^{-1}) $^7F_1$ 364, $^7F_2$ 895 and 1113, and $^5D_0$ 20 231. While the lower levels have an error of 12% or less, the $^5D_0$ level is 18% above the experimental value herein, and the T_{2g}−E_g splitting of $^7F_2$ is underestimated by 20%. This serves to demonstrate the simulation difficulties and inaccuracies of ab initio methods compared with crystal field parametrizations.

CONCLUSIONS

Two questions have been addressed in this article. First, since there are no abrupt changes in the luminescence spectrum on cooling from room temperature to 10 K, the luminescence probe of Eu^{3+} indicates that the structure of the Ba_2LnMO_6 systems is monoclinic. This conclusion is based upon the complete removal of cubic degeneracies, for example, in the $^5D_0 \rightarrow {}^7F_1$ transition, where 3 bands are observed. Furthermore, the dominance of the intensity of the $^5D_0 \rightarrow {}^7F_1$ transition in the emission spectrum shows that the Eu^{3+} ion is situated at a centrosymmetric site of C_{2h} or C_i symmetry. The appearance of the very weak $^5D_0 \rightarrow {}^7F_0$ transition is consistent with a slight distortion from centrosymmetry of the EuO_6 moiety, which could be due to crystal disorder. These results are in line with the crystal structure determinations of Henmi et al.[30] who concluded that the space group of these crystal systems is $P2_1/n$, which implies the site symmetry of C_i for the doped Eu^{3+} ion. The present results contrast with the previously reported emission spectrum of Ba_2LaNbO_6:Eu^{3+} where the forced electric dipole transition $^5D_0 \rightarrow {}^7F_2$ is dominant and the loss of centrosymmetry of Eu^{3+} is more apparent.[37] The vibrational spectra of Ba_2YNbO_6 show considerably more bands than those expected from the $Fm\bar{3}m$ space group, but at present, because

dx.doi.org/10.1021/jp303626v | J. Phys. Chem. A 2012, 116, 7337−7344

of computational limitations, we are unable to perform a DFT calculation using $P2_1/n$.

Although the presence of the impurities Cr^{3+} and Mn^{4+} in our samples severely limits the spectral information attainable, some conclusions have been made that relate the EuO_6^{9-} system in the context of other EuX_6^{3-} moieties. The empirical linear relationship between crystal field strength and electronegativity has been found for the $EuCl_6^{3-}$, EuO_6^{9-}, and EuF_6^{3-} moieties. While this can be qualitatively understood by the increase in covalency in the direction from the hexafluoro to the hexachloro systems, the wider applicability of this relationship and its theoretical justification are now the subject of further research.

AUTHOR INFORMATION

Corresponding Author

*E-mail: peter.a.tanner@gmail.com.

Notes

The authors declare no competing financial interest.

ACKNOWLEDGMENTS

Financial support from the National Science Foundation of China (Grant 11174005) is gratefully acknowledged by L.N.

REFERENCES

(1) Fu, W. T.; IJdo, D. J. W. *J. Solid State Chem.* **2006**, *179*, 1022.
(2) Lavat, A. E.; Baran, E. J. *Vibrat. Spectrosc.* **2003**, *2*, 167.
(3) Kurian, J.; Nair, K. V. O.; Sajith, P. K.; John, A. M.; Koshy, J. *Appl. Superconduct* **1998**, *6*, 259.
(4) Blasse, G.; Bril, A.; Nieuwpoort, W. C. *J. Phys. Chem. Solids* **1966**, *27*, 1587.
(5) Vijayakumar, C.; Padma Kumar, H.; Solomon, S.; Thomas, J. K.; Wariar, P. R. S.; John, A. *J. Alloys Compd.* **2009**, *480*, 167.
(6) Karunadasa, H.; Huang, Q.; Ueland, B. G.; Schiffer, B.; Cava, R. J. *Proc. Natl. Acad. Sci.* **2003**, *100*, 8097.
(7) Fujioka, Y.; Frantti, J.; Kakihana, M. *J. Phys. Chem. B* **2006**, *110*, 777.
(8) Kennedy, B. J.; Saines, P. J.; Kubota, Y.; Minakata, C.; Hano, H.; Kato, K.; Takata, M. *Mater. Res. Bull.* **2007**, *42*, 1875.
(9) Feldmann, D. M.; Holesinger, T. G.; Maiorov, B.; Foltyn, S. R.; Coulter, J. Y.; Apodaca, I. *Supercond. Sci. Technol.* **2010**, *23*, 095004.
(10) Chan, H. L. W.; Choy, S. H.; Chong, C. P.; Li, H. L.; Liu, P. C. K. *Ceram. Int.* **2008**, *34*, 773.
(11) Anderson, H. U. *Solid State Ionics* **1992**, *52*, 33.
(12) Tagantsev, A. K.; Sherman, V. O.; Astafiev, K. F.; Venkatesh, J.; Setter, N. *J. Electroceram.* **2003**, *11*, 5.
(13) Zhou, W.-L.; Zhang, Q.-L.; Gao, J.-Y.; Liu, W.-P.; Ding, L.-H.; Yin, S.-T. *Chin. Phys. B* **2011**, *20*, 016101.
(14) Eng, H. W.; Barnes, P. W.; Auer, B. M.; Woodward, P. M. *J. Solid State Chem.* **2003**, *175*, 94.
(15) Qi, X.; Gallagher, H. G.; Han, T. P. J.; Henderson, B.; Illingworth, B.; Ruddock, I. S. *Chem. Phys. Lett.* **1997**, *264*, 623.
(16) Kresse, G.; Furthmüller, J. *Phys. Rev. B* **1996**, *54*, 11169.
(17) Perdew, P.; Burke, K.; Ernzerhof, M. *Phys. Rev. Lett.* **1996**, *77*, 3865.
(18) Blöchl, P. E. *Phys. Rev. B* **1994**, *50*, 17953.
(19) Kresse, G.; Joubert, D. *Phys. Rev. B* **1999**, *59*, 1758.
(20) Dias, A.; Sá, R. G.; Moreira, R. L. *J. Raman Spectrosc.* **2008**, *39*, 1805.
(21) Moreira, R. L.; Abdul Khalam, L.; Sebastian, M. T.; Dias, A. *J. Eur. Ceram. Soc.* **2007**, *27*, 2803.
(22) Dias, A.; Khalam, L. A.; Sebastian, M. T.; Moreira, R. L. *J. Solid State Chem.* **2007**, *180*, 2143.
(23) Dias, A.; Abdul Khalam, L.; Sebastian, M. T.; Lage, M. M.; Matinaga, F. M.; Moreira, R. L. *Chem. Mater.* **2008**, *20*, 5253.
(24) Dias, A.; Lage, M. M.; AbdulKhalam, L.; Sebastian, M. T.; Moreira, R. L. *Chem. Mater.* **2011**, *23*, 14.
(25) Dias, A.; Abdul Khalam, L.; Sebastian, M. T.; Paschoal, C. W. A.; Moreira, R. L. *Chem. Mater.* **2006**, *18*, 214.
(26) Hammink, T. S.; Fu, W. T.; IJdo, D. J. W. *J. Solid State Chem.* **2011**, *184*, 848.
(27) Meneghini, C.; Ray, S.; Liscio, F.; Bardelli, F.; Mobilio, S.; Sarma, D. D. *Phys. Rev. Lett.* **2009**, *103*, 046409.
(28) Glazer, A. M. *Acta Crystallogr., Sect. A: Found. Crystallogr.* **1975**, *31*, 756.
(29) Howard, C. J.; Kennedy, B. J.; Woodward, P. M. *Acta Crystallogr., Sect. B: Struct. Sci.* **2003**, *59*, 463.
(30) Henmi, K.; Hinatsu, Y.; Masaki, N. M. *J. Solid State Chem.* **1999**, *148*, 353.
(31) Yashima, M.; Lee, J.-H.; Kakihana, M.; Yoshimura, M. *J. Phys. Chem. Solids* **1997**, *58*, 1593.
(32) Zhou, Q.; Kennedy, B. J.; Kimpton, J. A. *J. Solid State Chem.* **2011**, *184*, 729.
(33) Xiao, X. Z.; Yan, B. *J. Alloys Compd.* **2007**, *433*, 246.
(34) Yu, C. C.; Liu, X. M.; Yu, M.; Lin, C. K.; Li, C. X.; Wang, H.; Lin, J. *J. Solid State Chem.* **2007**, *180*, 3058.
(35) Werts, M. H. V.; Jukes, R. T. F.; Verhoeven, J. W. *Phys. Chem. Chem. Phys.* **2002**, *4*, 1542.
(36) Dutta, A.; Sinha, T. P. *Solid State Commun.* **2010**, *150*, 1173.
(37) Tanner, P. A.; Pan, Z. *Inorg. Chem.* **2009**, *48*, 11142.
(38) Liu, G. K. In *Spectroscopic Properties of Rare Earths in Optical Materials*; Liu, G. K., Jacquier, B., Eds.; Springer: Berlin, Germany, 2005; pp 1−89.
(39) Duan, C.-K.; Tanner, P. A. *J. Phys. Chem. A* **2010**, *114*, 6055.
(40) Görller-Walrand, C.; Binnemans, K. *Handbook on the Physics and Chemistry of Rare Earths*, Eds.; Gschneidner, K. A., Jr., Eyring, L.; Elsevier Science B. V.: Dordrecht, The Netherlands, 1996; Chapter 155, Vol. *23*, p 168.
(41) Cowan, R. D. *The Theory of Atomic Structure and Spectra*; University of California: Berkeley, CA, 1981.
(42) Shen, Y. R.; Holzapfel, W. B. *Phys. Rev. B* **1995**, *52*, 12618.
(43) Tanner, P. A.; Liu, Y.-L.; Edelstein, N.; Murdoch, K.; Khaidukov, N. M. *J. Phys.: Condens. Matter* **1997**, *9*, 7817.
(44) Tanner, P. A.; Li, W.; Ning, L. *Inorg. Chem.* **2012**, *51*, 2997.
(45) Barnes, J. C.; Al-Rasoul, K.; Harkins, P. *J. Chem. Soc. Pak.* **1980**, *2*, 9.
(46) Wakeshima, M.; Harada, D.; Hinatsu, Y.; Masaki, N. *J. Solid State Chem.* **1999**, *147*, 618.
(47) Auzel, F. *Mater. Res. Bull.* **1979**, *14*, 223.
(48) Auzel, F.; Malta, O. L. *J. Phys.* **1983**, *44*, 201.
(49) Thorne, J. R. G.; Jones, M.; McCaw, C. S.; Murdoch, K. M.; Denning, R. G.; Khaidukov, N. M. *J. Phys.: Condens. Matter* **1999**, *11*, 7851.
(50) Tanner, P. A.; Ravi Kanth Kumar, V. V.; Jayasankar, C. K.; Reid, M. F. *J. Alloys Compd.* **1994**, *215*, 349.
(51) McCaw, C. S.; Murdoch, K. M.; Denning, R. G. *Mol. Phys.* **2003**, *101*, 427.
(52) Visser, O.; Visscher, L.; Aerts, P. J. C.; Niewpoort, W. C. *J. Chem. Phys.* **1992**, *96*, 2910.